Apply Honey Badger Algorithm to double integral sliding mode observer for stable load frequency in multi-area power system

Anh-Tuan Tran[1], *Van Van Huynh*[2,*], *Thinh Lam-The Tran*[1]
[1]Faculty of Electrical and Electronics Engineering, Ton Duc Thang University, Ho Chi Minh City, Vietnam.
[2]Modeling Evolutionary Algorithms Simulation and Artificial Intelligence, Faculty of Electrical and Electronics Engineering, Ton Duc Thang University, Ho Chi Minh City, Vietnam.

*Corresponding Author: Van Van Huynh (email: huynhvanvan@tdtu.edu.vn)
(Received: 4-June-2024; accepted: 13-August-2024; published: 30-September-2024)
http://dx.doi.org/10.55579/jaec.202483.465

Abstract. *A randomness of load demand and plant uncertainties causes frequency deviation in linked power plants. Based on the double-integral sliding mode observer (DISMO) integrated Honey Badger algorithm (HBA), a novel LFC for a multi-area power plant (MAPP) is introduced in this article. The main aim is to minimize frequency offset, finite time, and aggregate instability of controllable loads subject to the balance of the power on the MAPP. Firstly, the suggested observer is developed to ensure an exact estimation of the actual signal for the controller input signal. Secondly, a double-integral sliding surface (DISS) is introduced based on estimated signals the designed observer gains. Then, a new SMC rule is designed to ensure finite time reachability and eliminate the chattering and oscillating troubles. Thirdly, in this regard, the proposed sliding surface is designed with four selected parameters. Regarding this, to maximize the ability of the suggested SMCer, the optimized controller parameters are determined by HBA. The robustness of the suggested scheme is examined by various case studies on the LFC models in a single-area power plant (SAPP) and MAPP under different load disturbances and parameter uncertainties.*

Keywords*: Honey Badger algorithm; Load frequency control; Electrical power plant; Sliding mode control.*

1. Introduction

In the power system, with non-stop development, the system schemes become complex due to the randomness of load demand, different electrical components, and plant uncertainties. Therefore, load frequency control (LFC) is not only mandatory to maintain stability but also one of the important problems in improving power quality. The key requirements of a stable PS are the ability to maintain good operation in the presence of load disturbances and plant uncertainties and to maintain the load frequency in the desired values [1, 2].

There are two major objectives of LFC including keeping the frequency of each area in the desired range and interchanged power between nearby areas within the allowable limit [3–5].

Various control approaches have been applied for LFC to deal with these control problems such as the PID method and its variation [6, 7], H-infinity control [8], Fuzzy logic algorithm [9], model predictive control [10], artificial intelligence techniques [11], and sliding mode control (SMC) [12–15], etc. Moreover, the most recent

methods applied for LFC in power systems were presented in [16–18].

SMC is well-known as one of the robust variable structure controls that help the system obtain high performance. Moreover, SMC is also non-sensitive to the change of the parameter uncertainty and load changes. Hence, SMC is widely applied in plenty of fields including non-linear systems [19], induction motors [20], wind turbines [21], converter systems [22], etc. However, the old-fashioned SMC exists some restrictions, so plenty of improved SMC methods have been proposed with different designs [23–26]. In [23], a first-order SMC is suggested to manage load frequency in MAPP under system parameter changes, EV reserves and time delay. However, this method still suffers chattering phenomenon. Therefore, in [24, 25], Guo. J and Huynh designed respectively the adaptive integral higher-order SMC and a second-order SMC via a DISS to free chattering and obtain a smooth control signal for MAPP under varying operating conditions. Although the designed controller is quite powerful and steady, these approaches are not very reliable because the sensors highly depend on the exact measurement of system state variables. Evidently, in a large-scale PS, the accurate measurement of all system states is not easy. In order to handle this problem, an SMC combined with an observer for the LFC of MAPP is suggested in [26].

Moreover, to optimize the effectiveness and robustness of the designed controller, many researchers have combined SMC with metaheuristic algorithms. By the way, to obtain the desired result, the SMC controller parameters are chosen by optimization algorithms [14, 27–30]. In [14], a higher-order SMC law based in integral sliding surface integrated HBA is introduced for MAPS under load disturbances and parameter uncertainties. In [27], a Bees algorithm is applied to tune the parameters of SMC regulated LFC in a two-area PS. Once again, in [28], Mokhtar et al suggested SMC based on LFC for Great Britain PS integrated Bees algorithm under load disturbances and parameter uncertainties. In addition, an SMC is continuously designed for LFC using Grey Wolf optimization to choose the controller parameters to gain the desired performance in [29]. Although the effectiveness of these schemes in studies [14, 27–29] is employed to the maximum by metaheuristic algorithms, it is still limited due to the proposed design only depending on integral sliding surface.

In this paper, a DISMO combined with HBA is designed for both SAPP and MAPP under step load changes. The proposed sliding surface has four parameters employed in the DISMC control law. The HBA technique is combined to gain the optimal performance for the proposed scheme. Finally, a DISS is employed fully based on the observer's estimated states to ensure this approach's high applicability.

The key contributions of this paper are listed below:

- The suggested controller is designed fully based on the observer's estimated local states and solve limitations of measurement.
- The new DISS is developed with 03 positive constants to eliminate the chattering and oscillating troubles that exist in integral SMC.
- To gain the best controller performance, both HBA and PSO methods have been employed to determine four controller parameters in each area.
- The proposed scheme is effective and powerful against system parameter uncertainties and step load changes.

2. Multi area power plant modelling

The suggested LFC based on SAPP and MAPP is shown in Fig. 1. Accordingly, this figure displays the model of an interconnected PS with the suggested controller employed by the combination between DISMO and HBA. From Fig. 1, the system equations in the area structure is

introduced below

$$\Delta\dot{F}_l = -\frac{1}{T_{Pl}}\Delta F_l + \frac{K_{Pl}}{T_{Pl}}\Delta P_{Ml} - \frac{K_{Pl}}{T_{Pl}}\Delta P_{Ll} - \frac{K_{Pl}}{T_{Pl}}\Delta P_{tie,lk} \quad (1)$$

$$\Delta\dot{P}_{Ml} = -\frac{1}{T_{Ml}}\Delta P_{Ml} + \frac{1}{T_{Ml}}\Delta P_{Vl} \quad (2)$$

$$\Delta\dot{P}_{Vl} = -\frac{1}{R_l T_{Vl}}\Delta F_l(t) - \frac{1}{T_{Vl}}\Delta P_{Vl}(t) + \frac{1}{T_{Vl}}\Delta P_{Cl} \quad (3)$$

$$\Delta\dot{E}_l = \beta_l K_{Il}\Delta F_l + K_{Il}\Delta P_{tie,lk} \quad (4)$$

$$\Delta\dot{\delta}_l = 2\pi\Delta F_l \quad (5)$$

where, ΔF_l, ΔP_{Vl}, ΔP_{Ml}, ΔE_l, and $\Delta\delta_l$ illustrate respectively the frequency variation, the mechanical power, the gate/valve position, the area control error, and finally, rotor angle deviations, $\Delta P_{tie,lk}$ illustrates the interconnected power, ΔP_{Cl} represents load demand change, ΔP_{Cl} illustrates control input. T_{Pl}, T_{Vl}, T_{Ml} illustrates respectively the power system time constants, governor, and steam. K_{Pl}, R_l, K_{Il}, β_l illustrate the power system gains. Finally, illustrates the tie-line coefficient. According to Eq. (1)-(5), the MAPP model can be revised as follows:

$$\dot{x}_l(t) = A_l x_l(t) + B_l u_l(t) + C_{lk} x_k + D_l \psi_l(t) \quad (6)$$

The system state variables of MAPP are displayed as follows

$$x_l(t) = \begin{bmatrix} \Delta F_l(t) & \Delta P_{Ml}(t) & \Delta P_{Vl}(t) & \Delta E_l(t) & \Delta\delta_l \end{bmatrix}^T$$

From the presented equations, we are able to identify the matrices A_l, B_l, C_{lk}, D_l as follows:

$$A_l = \begin{bmatrix} -\frac{1}{T_{Pl}} & \frac{K_{Pl}}{T_{Pl}} & 0 & 0 & -\frac{K_{Pl}}{T_{Pl}}\frac{1}{2\pi}T_{lk} \\ 0 & -\frac{1}{T_{Tl}} & \frac{1}{T_{Tl}} & 0 & 0 \\ -\frac{1}{R_1 T_{Vl}} & 0 & -\frac{1}{T_{Vl}} & 0 & 0 \\ K_{Il}\beta_1 & 0 & 0 & 0 & K_{Il}\frac{1}{2\pi}T_{lk} \\ 2\pi & 0 & 0 & 0 & 0 \end{bmatrix};$$

$$B_l = \begin{bmatrix} 0 \\ 0 \\ \frac{1}{T_{Vl}} \\ 0 \\ 0 \end{bmatrix}; C_{lk} = \begin{bmatrix} 0 & 0 & 0 & 0 & \frac{K_{Pl}}{T_{Pl}}\frac{T_{lk}}{2\pi} \\ 0 & 0 & 0 & 0 & 0 \\ 0 & 0 & 0 & 0 & 0 \\ 0 & 0 & 0 & 0 & -K_{Il}\frac{T_{lk}}{2\pi} \\ 0 & 0 & 0 & 0 & 0 \end{bmatrix};$$

$$D_l = \begin{bmatrix} -\frac{K_{Pl}}{T_{Pl}} \\ 0 \\ 0 \\ 0 \\ 0 \end{bmatrix}$$

In the actual power system, the measurement of the component values is difficult and costly. Therefore, parameters need to be estimated or calculated approximately. Also, state space form of PS is updated:

$$\begin{aligned} \dot{x}_l(t) &= \tilde{A}_l x_l(t) + \tilde{B}_l u_l(t) + \tilde{C}_{lk} x_k + \tilde{D}_l \psi_l(t) \\ &= A_l x_l(t) + B_l u_l(t) + C_{lk} x_k + w_l(t) \end{aligned} \quad (7)$$

where $\tilde{A}_l = A_l + \Delta A_l, \tilde{D}_l = D_l + \Delta D_l, \tilde{C}_l = C_l + \Delta C_l, \tilde{B}_l = B_l + \Delta B_l$ and the unknown matrices $\Delta A_l(x), \Delta B_l(t)$ indicate by system deviation, the matrices A_l, B_l , C_{lk} and D_l are the nominal values; $w_l(t)$ is assumed the total disturbances estimated as below:

$$w_l(t) = \Delta A_l x_l(t) + \Delta B_l u_l(t) + \Delta C_{lk} x_k(t) + \tilde{D}_l \psi_l(t) \quad (8)$$

The ideal situation, some lemmas and assumption are presented in this part to illustrate the stability and feasibility of the PS and the parameters-based LFC schemes over various conditions,

Assumption 1: If the matrix A_l, B_l is controllable then $\Delta A_l(t), \Delta B_l(t)$ can be estimated.

Lemma 1 [26]: Let Y and X are realistic matrices with suitable dimensions, for any scalar $\mu > 0$, the below matrix inequality is achieved.

$$X^T Y + Y^T X \leq \mu X^T X + \mu^{-1} Y^T Y. \quad (9)$$

Lemma 2 [26]: If the matrix:

$$\begin{bmatrix} P(x) & R(x) \\ R^T(x) & Q(x) \end{bmatrix} > 0$$

where $P(x) = P^T(x), Q(x) = Q^T(x)$ and $R(x)$ which depends on x. Hence, $Q(z) > 0$ and $P(x) - R(x)Q^{-1}(x)R^T(x) > 0$.

3. Double-integral SMC based state observer

In MAPS, a DISMO is combined with HBA to maximize frequency controller performance. A suggested observer is designed to correctly estimate all state values completely based on system input and output. Simultaneously, a DISMC is designed to improve the closed-loop system's performance.

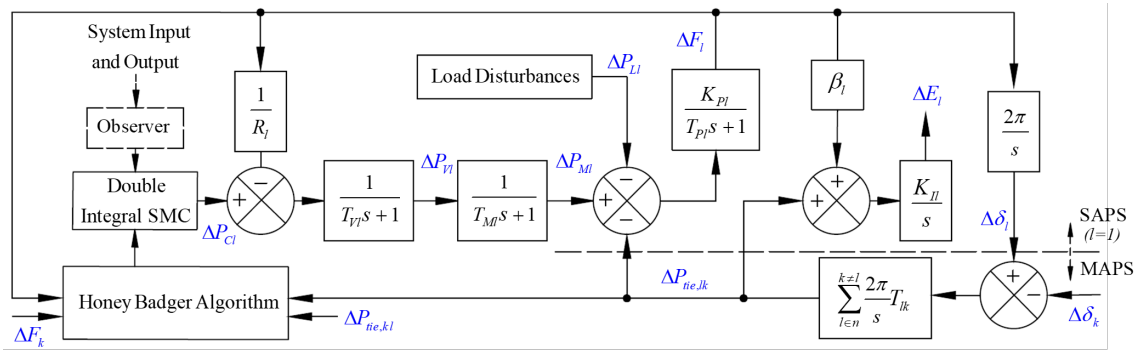

Fig. 1: The structure of LFC model of MAPP.

3.1. The observer structures

In MAPP, the measurements of all system state variables become more difficult and complex. In this part, the state observer is introduced to solve the estimating and observing all system states [28]. The observer state-space equation is determined below.

$$\begin{aligned}\dot{\hat{x}}_l(t) &= A_l\hat{x}_l(t) + B_l u_l(t) + C_{lk}\hat{x}_k(t) + L_l[y_l(t) - \hat{y}_l(t)]\\ \hat{y}_l(t) &= F_l\hat{x}_l(t)\end{aligned} \tag{10}$$

To get the optimal performance in estimation, we calculate observer gain (H_l) via pole placement approach [26] which leads the eigenvalues $(A_l^T - C_l^T H_l)$ to be placed in the negative hyper plane. The matrix observer gain (L_l) can be selected by using: $L_l = (H_l)^T$.

Assumption 2: Eigenvalues of $(A_l - L_l F_l)$ could be chosen by suitable choice of (L_l) when the matrices pair $[A_l, F_l]$ is observable.

3.2. The double-integral SMC design based on state observer.

This part introduces the structure of a DISMO based on LFC in a MAPS. Accordingly, it enhances the PS performance by maintain a steady frequency according to a random disturbance. Also, the DISMC enhances the transient and steady-state response with mismatched and matched uncertainties [26] or even maintain the PS in steady-state in the presence of non-linear uncertainties such as GRC [30].

Then, we suggest the double integral sliding surface for the MAPP below:

$$\begin{aligned}\sigma_l(\hat{x}_l, t) = \varepsilon_{l1} G_l\hat{x}_l(t) - \varepsilon_{l2} G_l \int_0^t (A_l - B_l K_l)\hat{x}_l(\tau)d\tau\\ - \varepsilon_{l3}\int_0^t\int_0^t G_l(A_l - B_l K_l)\hat{x}_l(\tau)d\tau d\tau\end{aligned} \tag{11}$$

where ε_{l1} and ε_{l2} are the positive constants, G_l, K_l are the designed matrices. G_l is chosen to ensure that $G_l B_l$ is invertible.

Remark 1: K_l is determined by using the pole placement technique [26] which leads the eigenvalues $(A_l - B_l K_l)$ to be selected in the negative hyper plane. Differentiate $\sigma_l(\hat{x}_l, t)$ in Eq. (12) and combined with Eq. (11), we have:

$$\begin{aligned}\dot{\sigma}_l(\hat{x}_l, t) &= (\varepsilon_{l1} - \varepsilon_{l2})G_l A_l\hat{x}_l(t) + \varepsilon_{l1} G_l B_l u_l(t)\\ &+ \varepsilon_{l1} G_l C_{lk}\hat{x}_k(t) + \varepsilon_{l1} G_l L_l[y_l(t) - \hat{y}_l(t)]\\ &+ \varepsilon_{l2} G_l B_l K_l\,\hat{x}_l(t) - \varepsilon_{l3}\int_0^t G_l(A_l - B_l K_l)\hat{x}_l(\tau)d\tau\end{aligned} \tag{12}$$

In order to obtain the MAPS stability, displayed as (11), the DISMO law is introduced as follows

$$u_l^{DISMO}(t) = u_l^{eq}(t) + u_l^{SW}(t) \tag{13}$$

where,

$$\begin{aligned}u_l^{eq}(t) &= -(\varepsilon_{l1} G_l B_l)^{-1}\{(\varepsilon_{l1} - \varepsilon_{l2})G_l A_l\hat{x}_l(t)\\ &+ \varepsilon_{l1} G_l C_{lk}\hat{x}_k(t) + \varepsilon_{l1} G_l L_l[y_l(t) - \hat{y}_l(t)]\\ &- \varepsilon_{l2} G_l B_l K_l\hat{x}_l(t) - \varepsilon_{l3}\int_0^t G_l(A_l - B_l K_l)\hat{x}_l(\tau)d\tau\}\end{aligned} \tag{14}$$

and

$$u_l^{SW}(t) = -(\varepsilon_{l1} G_l B_l)^{-1}\delta_l\, sat(\sigma_l[\hat{x}_l(t)]) \tag{15}$$

where $\delta_l > 0$ and

$$\mathrm{sat}(\text{œ}_\mathrm{l}[\hat{\mathrm{x}}_\mathrm{l}(\mathrm{t})]) = \begin{cases} 1, & \sigma_l[\hat{x}_l(t)] > 1 \\ \sigma_l[\hat{x}_l(t)], & \text{when } -1 \le \sigma_l[\hat{x}_l(t)] \le 1 \\ -1, & \sigma_l[\hat{x}_l(t)] < -1 \end{cases}$$

Proof: Constructing a Lyapunov function

$$V(t) = \sum_{l=1}^{N} \|\sigma_l[\hat{x}_l(t)]\| \tag{16}$$

So, derivative $V(t)$ in (16), that we have

$$\begin{aligned} \dot{V}(t) = & \sum_{l=1}^{N} \frac{\sigma_l^T[\hat{x}_l(t)]}{\|\sigma_l[\hat{x}_l(t)]\|}[(\varepsilon_{l1} - \varepsilon_{l2})G_l A_l \hat{x}_l(t) \\ & + G_l \varepsilon_{l1} B_l u_l(t) + G_l \varepsilon_{l1} C_{lk} \hat{x}_k(t) \\ & + G_l \varepsilon_{l1} L_l[y_l(t) - \hat{y}_l(t)] - G_l \varepsilon_{l2} B_l K_l \, \hat{x}_l(t) \\ & + \sum_{l=1}^{N} [\frac{\sigma_l^T[\hat{x}_l(t)]}{\|\sigma_l[\hat{x}_l(t)]\|} \varepsilon_{l1} G_l B_l u_l(t) \end{aligned} \tag{17}$$

Substituting u_l^{DISMO} in (14) into $\dot{V}(t)$ in (17), we gain

$$\dot{V}(t) = -\sum_{l=1}^{N} \delta_l \, \|\sigma_l[\hat{x}_l(t)]\| \tag{18}$$

The above inequality implies that the system trajectories of the DISMC law (11) reach the sliding surface $\sigma_l[\hat{x}_l(t)]$ and keep it for later.

3.3. Stability analysis

The stability of MAPP is illustrated in this part. The proposed scheme concentrates on ultimate edge of whole interest signals. The ultimate edge can be determined by the suitable choice of controller parameters without information of the uncertainty edge.

It can be observed that $\dot{V}(t) \le 0$. We have

$$\dot{V}(t) \le \dot{V}(0) \le \sum_{l=1}^{N} \|\sigma_l[\hat{x}_l(0)]\| \tag{19}$$

And then, combining the second derivative of $V(t)$ and Eq. (16), (18), and (19), we have

$$\ddot{V}(t) \le {\delta_l}^{-2} e^{-\delta_l t} V(0) \tag{20}$$

where $\bar{\delta}_l = Min\,(\delta_l)$ and $n = 1, 2, .., N$.

Limiting t reaches infinity on two sides of (20), it can be displayed below.

$$\lim_{t\to\infty} \ddot{V}(t) \le {\delta_l}^{-2} e^{-\delta_l t} V(0) = 0 \tag{21}$$

It is easy to realize that $\ddot{V}(t)$ is bounded. Thus, $\dot{V}(t)$ is continuous. Accordingly, prove from equations (18), (19), and (13) that $V(t)$ is bounded and $\dot{V}(t)$ is negative semi-definite. By employing Barbalats (or the Lyapunov-like lemma) [31] (18), (19), and (21), we have

$$\lim_{t\to\infty} \dot{V}(t) = \lim_{t\to\infty} [-\sum_{l=1}^{N} \delta_l \, \|\sigma_l[\hat{x}_l(t)]\|] = 0 \tag{22}$$

It is clearly that $\lim_{t\to\infty} \sigma_l[\hat{x}_l(t)] = 0$. Hence, by standard linear control argument, $\lim_{t\to\infty} \hat{x}_l(t) = 0$ is obtained and the asymptotic stability of the MAPS can be ensured.

Remark 1: Unlike with the traditional integral sliding surface given in [14], the double integral sliding surface combined with HBA is designed for both SAPP and MAPP to improve the SAPP and MAPP's transient performance.

4. Honey badger algorithm

HBA is a new nature-inspired meta-heuristic algorithm, it was designed based on mimicking the hunting behavior of Honey Badger swarm. HBA performance is superior to other algorithms proposed before such as PSO, SA, L-SHADE, MFO, CMA-ES, GOA, WOA, TEO and HHO while examined by four engineering design problems in practice and CEC'17 serial benchmark functions.

The main difference between HBA and other algorithms in the same class is the update process for new solutions as presented detail in paper [14]. Accordingly, there are two main stages to this process, including 1. *Ditch creating stage* and 2. *Honey flavor guided stage*. Two stages will be illustrated in the sub-sections below.

4.1. Ditch creating stage

This stage is to support the honey badger in identifying the prospect prey position in a specific area by employing its smelling ability. Meanwhile, the honey badger position is continuously changed to get closer to the prey. This behavior is shown by the equation as below:

$$S_n^{new} = S_{pp} + RI \times DF \times C\mathrm{S} \times S_{pp} + RI \times r\mathrm{d}_3 \times \varepsilon \times l_l \left|\cos(2\pi d_4) \times [1 - \cos(2\pi d_4)]\right| \quad (23)$$

and

$$RI = \begin{cases} 1 if rd_6 \le 0.5 \\ -1, otherwise \end{cases} \quad (24)$$

where RI is the reference information; DF is the degree of having food while honey badger engages the hunting process. By experiments, the value of DF is greater than 1 and DF is set by 6 in HBA; rd_3, rd_4 and rd_5 are the random values generated in the interval between 0 and 1, respectively.

4.2. The honey flavor guided stage

The honey badger will combine with a navigator called a honeyguide bird to increase the probability of success while searching for a honey barge in a large-scale area. This kind of bird will bring the honey badger to the point where the beehive is located. This collaboration is illustrated by following equation.

$$S_n^{new} = S_{pp} + RI \times r\mathrm{d}_7 \times \varepsilon \times l_i \quad (25)$$

where, rd_7 is a random value generated in the interval between 0 and 1.

The whole computing execution of HBA can be described by the flowchart in Fig 2:

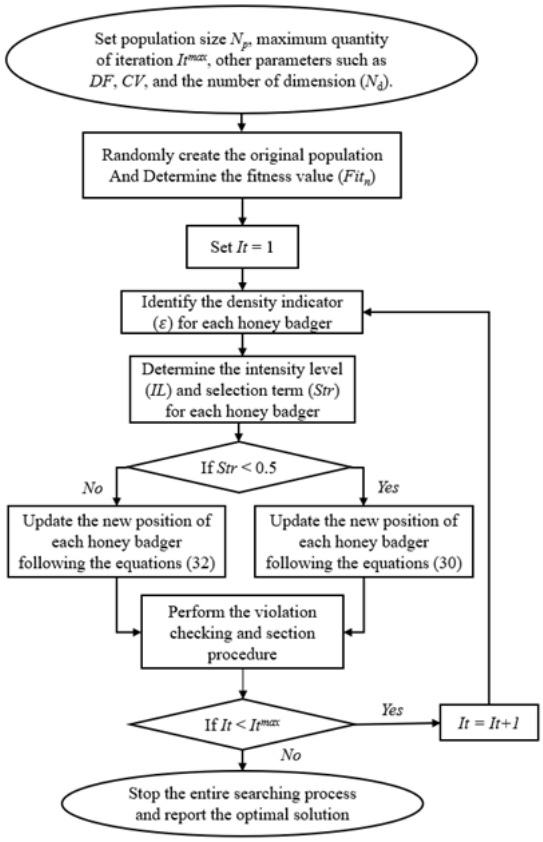

Fig. 2: The entire searching process of HBA for a typical optimization problem [14].

5. The implementation of the methods for the dismo controller design problem

In this part, the implementation of HBA will be employed to determine the optimized parameters for the DISMO controller. The crucial parameters needed to identify an optimal controller include $\varepsilon_{l1}, \varepsilon_{l2}, \varepsilon_{l3}$ and δ_l. The diagram of the algorithm according to the control scheme is depicted in Fig. 3:

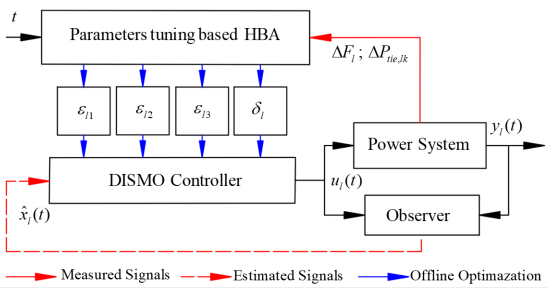

Fig. 3: The block diagram of the HBA based DISMO scheme.

The real performance of meta-heuristic methods will be evaluated for the purpose of shorten-

ing the overshoot accompanied by settling time. In order to reach that goal, the minimizing of Integral Time Absolute Error (ITAE) is utilized to be the main objective function, detailed as follows:

$$ITAE_{MAPS} = \int_0^{t_{sim}} \sum_{l=1}^{N} (|\Delta F_l| + \sum_{l=n(k\neq l)}^{N} |\Delta P_{tie,lk}|) \times t \times dt \quad (26)$$

where t and t_{sim} is real-time and total simulation time respectively.

6. Simulation results

In this part, the two case studies for SAPP and MAPP are performed to assess the robustness of the proposed controller under step load changes. In addition, to illustrate the superiority, the results are employed to compare with other schemes under Max(ΔF_l) and settling time.

6.1. SAPP

The parameter of SMC is optimized HBA and PSO techniques. The convergence curves on 50 iterations based on fitness value are illustrated in Fig. 4 for SAPS. The optimal parameters of DISMO controller optimized by PSO and HBA for SAPS are displayed in Table 1. The system parameters and step load change of single area [14,32] are presented respectively as follows: $K_p = 1, T_p = 10, T_t = 0.3, T_g = 0.1, K_e = 50, \beta = 0.4$ and load disturbances is employed with +0.16 pu at 1s. Accordingly, Fig. 4, Fig. 6 display the best convergence curves gained by HBA/PSO and frequency deviation achieved by proposed, respectively. As shown in Fig. 6, it is easy to observe that the suggested DISMO controller reduces the peak-value of frequency variation and maximum settling time compared with other schemes. The detailed values of overshot and settling time of each method are presented in Table 2. The robustness and efficiency of LFC against the different load disturbances can be enhance be employing the suggest scheme.

Tab. 1: Optimal parameters for SAPS.

Method	Parameters	SAPS
HBA-DISMO	ε_1	49.900
	ε_2	39.2293
	β_1	10.6728
	δ_1	0.1000
PSO-DISMO	ε_1	49.900
	ε_2	32.0387
	β_1	2.2219
	δ_1	49.900

In addition, Fig. 5 illustrates the actual and estimated signals. Accordingly, the simulation results indicate that the designed observer produces an exact estimation completely based on system output and input.

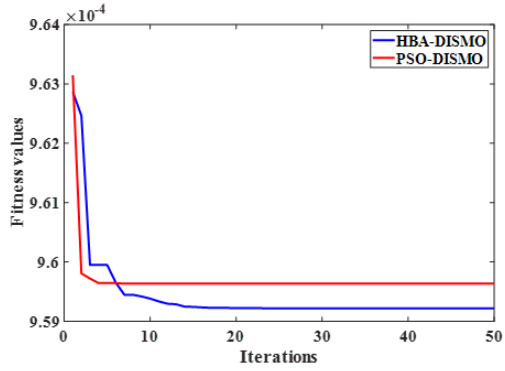

Fig. 4: The best fitness value on 50 iterations SAPS.

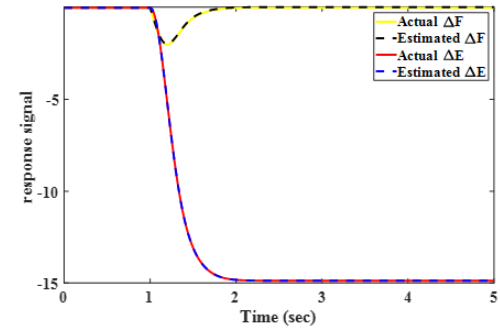

Fig. 5: Actual and estimated response signals of the suggested controller.

6.2. TAPP

The parameters of TAPS [14, 32] are presented as follows: $T_{p1} = 10, T_{p2} = 8, K_{p1} = 1, K_{p2} =$

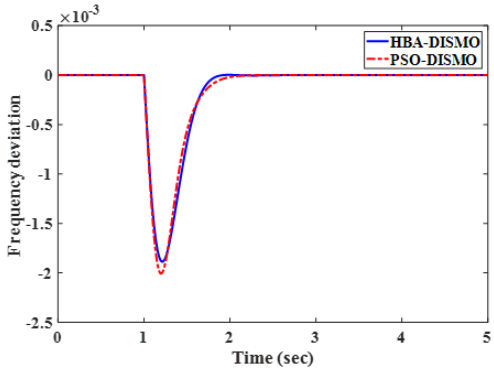

Fig. 6: The frequency variation.

Tab. 2: The sum of absolute itae function and frequency deviation in SAPS.

Method	Proposed SMC	PSO-DISMC	PSO-DHOSMC	HBA-DHOSMC
ITAE_{SAPS}	0.009592	0.009596	0.0136	0.0133
$\lvert\Delta F\rvert$	1.887×10^{-3}	2.007×10^{-3}	2.34×10^{-3}	2.15×10^{-3}

$6.67, T_{g1} = 0.1, T_{g2} = 0.17$, $K_{e1} = 0.1, K_{e2} = 0.1, T_{t1} = 0.3, T_{t2} = 0.4, R_1 = R_2 = 0.055$ and $\beta_1 = \beta_2 = 0.4$. A step load change is assumed for the first area with values as +0.1 p.u. at 1s. In this case, to resemble the modern PS situation, we consider further the wind turbine plant effect as a flexible power sources for assessing the effectiveness of suggested scheme. Accordingly, the output power change of wind turbine is illustrated in Fig. 8. The best fitness values are displayed in Fig. 7, it is easy to realize that while optimizing for large systems with many involving variables, the superiority of HBA to PSO [14] is more vivid. Fig. 10 displayed tie-line power of the two areas. The values of frequency fluctuation in areas 1 and 2 are illustrated in Fig. 9.

Tab. 3: Optimal parameters for TAPP.

Method	Parameter	First area	Second area
HBA-DISMO	ε_{l1}	0.1266	19.5387
	ε_{l2}	0.100	8.9526
	ε_{l3}	1.1041	47.2014
	δ_l	0.1000	0.1000

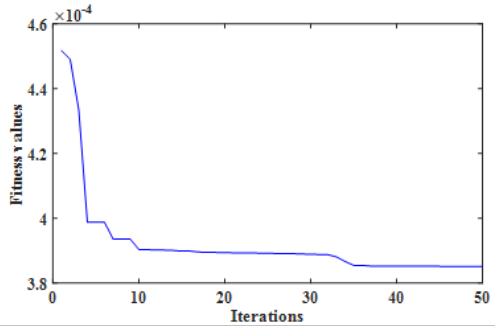

Fig. 7: The best fitness value on 50 iterations of TAPS.

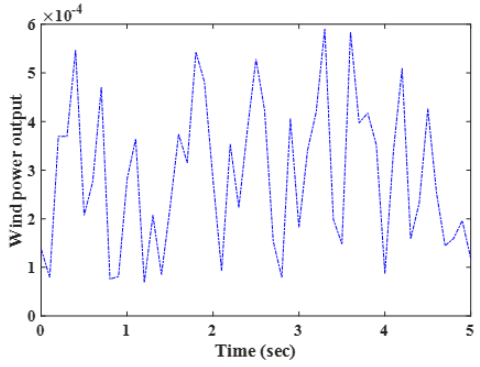

Fig. 8: The output power of wind turbine.

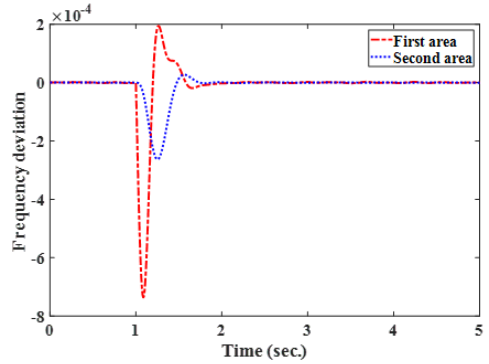

Fig. 9: The frequency variation.

6.3. Discussion

In 6.1 and 6.2 sections, both single and two-area PS were employed to assess the effectiveness and robustness of suggested scheme under uncertainties and step load change. Based on local states estimated by designed observer, the suggested controller is simple to apply for realistic system. In addition, double integral slid-

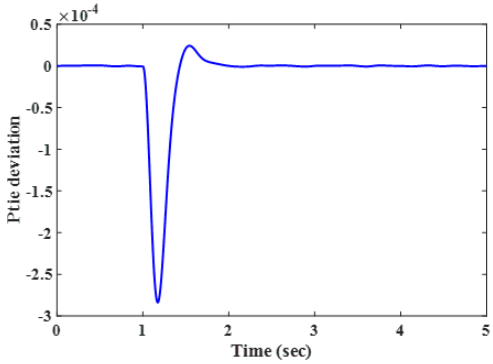

Fig. 10: The Tie-line power variation.

ing surface is designed to optimal avoid chattering which is known as key drawback of traditional SMC. Finally, using HBA for fine-tune optimal parameters, which are given in Table 3, also brings a superior performance for controller. The simulated results show that the suggested approach can dramatically reduce tie-line power and frequency variation. Accordingly, DISMC integrated HBA has achieved the ITAE value at 0.009592 and 3.85×10^{-4} for single and two-area PS, respectively that lowest value when compared with other methods, as given in Table 4.

Tab. 4: The sum of absolute itae function and response signals in mapp.

Method	Proposed SMC	HBA-dHoSMC
ITAE_{MAPP}	3.85×10^{-4}	6.45×10^{-4}
$\lvert\Delta F_1\rvert$	7.37×10^{-4}	7.92×10^{-4}
$\lvert\Delta F_2\rvert$	2.63×10^{-4}	2.66×10^{-4}
$\lvert\Delta P_{tie,12}\rvert$	2.84×10^{-4}	4.59×10^{-4}

7. Conclusion

This study introduces a DISMO-integrated HBA for a MAPP under step load disturbances. First, the suggested observer is used to estimate exactly only local state variables based on system input and output. Therefore, the suggested controller is relatively easy for practical implementation. Second, the new DISMC is designed to avoid optimally chattering issues in traditional techniques. In terms of the suggested controller design, the HBA technique was also further developed for maximum improvement of controller performance. The simulated results emphasize that the suggested scheme has better control performance than other schemes.

For future work, we will examine the robustness of the proposed approach with the complex PS including different sources and renewable energy sources. In addition, the energy storage system will also be employed to improve the LFC loop.

Acknowledgment

This research is funded by Ton Duc Thang University under grant number <FOSTECT.2022.04>.

References

[1] L. L. Grigsby. Power system stability and control. *CRC press*, 2007.

[2] H. Bevrani. Robust power system frequency control. *Springer-Verlag US*, 2009.

[3] E. M. Ahmed, E. A. Mohamed, A. Selim, M. Aly, A. Alsadi, W. Alhosaini, H. Alnuman, and H. A Ramadan. Improving load frequency control performance in interconnected power systems with a new optimal high degree of freedom cascaded fotpid-tidf controller. *Ain Shams Eng. J.*, 14:102207, 2023.

[4] N. Ram Babu, S. K. Bhagat, L. C. Saikia, T. Chiranjeevi, R. Devarapalli, and F. P García Márquez. A comprehensive review of recent strategies on automatic generation control/load frequency control in power systems. *Arch. Comput. Methods Eng.*, 30:543–572, 2023.

[5] S. Kumari and P. K Pathak. A state-of-the-art review on recent load frequency control architectures of various power system configurations. *Electr. Power Components Syst.*, 52:722–765, 2024.

[6] M. Cui, Y. Zhao, P. Cao, Y. Tang, and Y Lu. Load frequency control of interconnected hydrothermal power system based on fopi+ fopd controller. *Int. J. Dyn. Control.*, 12:1073–1085, 2024.

[7] M. A. Metwally, M. A. Ali, S. A. Kutb, and F. M Bendary. A genetic algorithm for optimum design of pid controller in multi area load frequency control for egyptian electrical grid. *Int. J. Eng. Res. & Technol. (IJERT)*, 5:267–275, 2016.

[8] Q. Zhong, J. Yang, K. Shi, S. Zhong, Z. Li, and M. A Sotelo. Event-triggered h∞ load frequency control for multi-area nonlinear power systems based on non-fragile proportional integral control strategy. *IEEE Trans. on Intell. Transp. Syst.*, 23:12191–12201, 2021.

[9] A. M. A. Soliman, M. Bahaa, and M. A Mehanna. . pso tuned interval type-2 fuzzy logic for load frequency control of two-area multi-source interconnected power system. *Sci. Reports*, 13:8724, 2023.

[10] M. A. Mohamed, A. A. Z. Diab, H. Rezk, and T. Jin. A novel adaptive model predictive controller for load frequency control of power systems integrated with dfig wind turbines. *Neural Comput. Appl.*, 32:7171–7181, 2020.

[11] Y. Zheng, J. Tao, Q. Sun, Chen Sun, H., Z., and M Sun. Deep reinforcement learning based active disturbance rejection load frequency control of multi-area interconnected power systems with renewable energy. *J. Frankl. Inst.*, 360:13908–13931, 2023.

[12] A. T. Tran, B. Le Ngoc Minh, P. T. Tran, V. V. Huynh, V. D. Phan, V. T. Pham, and T. M. Nguyen. Adaptive integral second-order sliding mode control design for load frequency control of large-scale power system with communication delays. *Complexity*, 2021:1–19, 2021.

[13] J. Guo. Application of full order sliding mode control based on different areas power system with load frequency control. *ISA transactions*, 92:23–34, 2019.

[14] T. Tran, M. P. Duong, N. T. Pham, and J. W Shim. Enhanced sliding mode controller design via meta-heuristic algorithm for robust and stable load frequency control in multi-area power systems. *IET Gener. Transm. & Distribution*, 18:460–478, 2024.

[15] A. Dev and M. K. Sarkar. Robust higher order observer based non-linear super twisting load frequency control for multi area power systems via sliding mode. *Int. J. Control. Autom. Syst.*, 17:1814–1825, 2019.

[16] M. S. Alam, T. A. Chowdhury, A. Dhar, F. S. Al-Ismail, M. S. H. Choudhury, M. Shafiullah, and S. M Rahman. Solar and wind energy integrated system frequency control: A critical review on recent developments. *Energies*, 16:812, 2023.

[17] I. A. Khan, H. Mokhlis, N. N. Mansor, H. A. Illias, L. J. Awalin, and L Wang. New trends and future directions in load frequency control and flexible power system: A comprehensive review. *Alex. Eng. J.*, 71:263–308, 2023.

[18] M. Wadi, A. Shobole, W. Elmasry, and I Kucuk. Load frequency control in smart grids: A review of recent developments. *Renew. Sustain. Energy Rev.*, 189:114013, 2024.

[19] S. Mobayen, F. Bayat, S. Din, and M. T Vu. Barrier function-based adaptive nonsingular terminal sliding mode control technique for a class of disturbed nonlinear systems. *ISA transactions*, 134:481–496, 2023.

[20] H. H. Vo. Sensorless induction motor drive using modified integral sliding mode control-based mras. *J. Control. Eng. Appl. Informatics*, 25:45–54, 2023.

[21] R. Venkateswaran, A. A. Yesudhas, S. R. Lee, and Y. H Joo. Integral sliding mode control for extracting stable output power and regulating dc-link voltage in pmvg-based wind turbine system. *Int. J. Electr. Power & Energy Syst.*, 144:108482, 2023.

[22] J. Wu and Y. Lu. Adaptive backstepping sliding mode control for boost converter

with constant power load. *IEEE Access*, 7:50797–50807, 2019.

[23] H. H. Alhelou, N. Nagpal, N. Kassarwani, and P Siano. Decentralized optimized integral sliding mode-based load frequency control for interconnected multi-area power systems. *IEEE Access*, 11:32296–32307, 2023.

[24] J Guo. The load frequency control by adaptive high order sliding mode control strategy. *IEEE Access*, 10:25392–25399, 2022.

[25] V. Van Huynh, P. T. Tran, C. S. T. Dong, B. D. Hoang, and O Kaynak. Sliding surface design for sliding mode load frequency control of multiarea multisource power system. *IEEE Trans. on Ind. Informatics*, 20:7797–7809, 2024.

[26] A. T. Tran, N. T. Pham, V. Van Huynh, and D. N. M Dang. Stabilizing and enhancing frequency control of power system using decentralized observer-based sliding mode control. *J. Control. Autom. Electr. Syst.*, 34:541–553, 2023.

[27] M. Shouran, F. Anayi, and M Packianather. The bees algorithm tuned sliding mode control for load frequency control in two-area power system. *Energies*, 14:5701, 2021.

[28] M. Shouran, F. Anayi, and M. Packianather. Design of sliding mode control optimised by the bees algorithm for lfc in the great britain power system. *Mater. Today: Proc.*, 52:937–943, 2022.

[29] A. Kumar, M. N. Anwar, and S. Kumar. Sliding mode controller design for frequency regulation in an interconnected power system. *Prot. Control. Mod. Power Syst.*, 6:1–12, 2021.

[30] M.A.E. Mohamed, S.M.R. Mohamed, E.M.M. Saied, M. Elsisi, C.L. Su, and H.A. Hadi. Optimal energy management solutions using artificial intelligence techniques for photovoltaic empowered water desalination plants under cost function uncertainties. *IEEE Access*, 10:93646–93658, 2022.

[31] J. J. E. Slotine and W Li. Applied nonlinear control. *Englewood Cliffs, NJ: Prentice hall*, 199, 1991.

[32] C. Mu, Y. Tang, and H. He. Improved sliding mode design for load frequency control of power system integrated an adaptive learning strategy. *IEEE Trans. on Ind. Electron.*, 64:6742–6751, 2017.

About Authors

Anh-Tuan TRAN received B.Eng. degree in Electrical and Electronics Engineering, and M.Eng. degree in Electrical Engineering at Ton Duc Thang University (TDTU), Ho Chi Minh City, Vietnam in 2019 and 2021 respectively. At present, he is a member of Modeling Evolutionary Algorithms Simulation and Artificial Intelligence, Faculty of Electrical & Electronics Engineering, Ton Duc Thang University. His areas of interest include power system dynamics, stability and control; Energy storage system; Sliding mode control, observer, LQG; Optimization algorithms.

Van Van HUYNH received the Ph.D. degree in mechanical and automation engineering from Da-Yeh University, Changhua, Taiwan, in 2015. He is currently a Lecturer with the Faculty of Electrical and Electronics Engineering, Ton Duc Thang University, Ho Chi Minh City, Vietnam. His current research interests include sliding mode control, variable structure control, and power system control.

Thinh Lam-The TRAN was born in Ca Mau City, Vietnam. Currently, he is B.Eng. student in Electrical Engineering, Ton Duc Thang University, Ho Chi Minh City, Vietnam. His research topics included load frequency control, sliding mode control and optimal control.